Bulk Properties and Transport Mechanisms of Solid State Antiperovskite Li-ion Conductor Li_3OCl : Insights from First Principles Calculations—Supplementary Information

Musheng Wu[a], Bo Xu[a], Xueling Lei[a], Kelvin Huang[b], Chuying Ouyang*[a]

[a] *Department of Physics, Laboratory of Computational Materials Physics, Jiangxi Normal University, Nanchang, China*

[b] *Department of Mechanical Engineering, University of South Carolina, Columbia, USA*

E-mail: cyouyang@jxnu.edu.cn

1. Detailed calculations

For primitive cell optimization and elastic property calculations, a 6×6×6 Monkhorst-Pack[1] *k*-point grid in the Brillouin Zone is sampled. The convergence criteria for the total energies and ionic forces are set to 10^{-5} eV and 10^{-3} eV/Å, respectively. For the density of states (DOS) calculations, a 12×12×12 *k*-mesh is used, and the Gaussian smearing method with a smearing width of 0.05 eV is used. The Heyd-Scuseria-Erznerhof (HSE06)[2] hybrid functional is used to calculate the band structure of Li_3OCl. In terms of band gaps calculations, hybrid Hartree-Fock/DFT approaches[3] are used since it has been proven more reliable than the GGA-PBE functional.

For phonon data calculations, the PHONOPY code is used for the calculation of the phonon dispersion spectrum and thermodynamic properties,[4] which directly uses the dynamic matrices calculated by the density functional perturbation theory (DFPT)[5] implemented in VASP. A 4×4×4 *k*-point grid and 10^{-8} eV/Å electronic forces convergence are used. For defects formation energy and Li^+ migration energy barrier calculations, a 3×3×3 supercell of the primitive cubic-unit cell (containing 135 atoms) is used with a 2×2×2 *k*-point grid and 5×10^{-2} eV/Å ionic forces convergence. The Li^+ migration energy barriers are obtained using

the climbing image nudged elastic band (CI-NEB) method,[6] which optimizes the migration pathway and determines the saddle points along Li^+ migration pathway.[7]

2. Mechanical properties

The bulk modulus and shear modulus can be obtained by the following expression [8]

$$B_V = B_R = \frac{C_{11} + 2C_{12}}{3}, \quad (1)$$

$$G_V = \frac{C_{11} - C_{12} + 3C_{44}}{5}, \text{ and } G_R = \frac{5(C_{11} - C_{12})C_{44}}{4C_{44} + 3(C_{11} - C_{12})}. \quad (2)$$

where B_V, B_R and G_V, G_R, are bulk moduli and shear moduli obtained from the Voigt (*V*) [9] or Reuss (*R*) [10] schemes, respectively; C_{11}, C_{12}, and C_{44} are the independent elastic constants.

However, the upper and lower limits of the polycrystalline bulk and shear modulus can be obtained by Voigt and Reuss schemes, respectively. Therefore, in the present work, to obtain accurately elastic moduli, the Voigt-Reuss-Hill approximations [11] are applied to estimate the average bulk (*B*) and shear (*G*) modulus in the following expressions

$$B = \frac{B_V + B_R}{2}, \quad (3)$$

$$G = \frac{G_V + G_R}{2}, \quad (4)$$

where *B* represents the resistance to volume change by an applied pressure; *G* is the opposition to reversible shear deformations. Generally speaking, *G* can better predict the hardness of a material than *B*. Furthermore, the value of *B/G* (known as the Pugh's ratio) is generally used to evaluate the ductility/brittleness nature of materials based on the Pugh's criterion.[12] When the B/G ratio is larger than 1.75, the material is regarded as ductile; otherwise it is brittle.

From the obtained *B* and *G*, other elastic parameters, *i. e.* Young's modulus (*E*) and Poisson's ratio (*v*), can be calculated by the following expression[8]

$$E = \frac{9BG}{3B + G}, \tag{5}$$

$$v = \frac{3B - 2G}{2(3B + G)}. \tag{6}$$

In addition, a dimensionless quantity A_G representing the degree of elastic anisotropy in shear for the cubic crystal is also calculated by [13]

$$A_G = \frac{G_V - G_R}{G_V + G_R}, \tag{7}$$

A_G is zero for the elastically isotropic crystals. The larger the value A_G, the higher the elastic anisotropy of crystals.

3. Thermodynamic properties

3.1 Thermal expansion coefficient

To obtain the volume thermal expansion coefficient (α_V) of cubic Li_3OCl, we calculated the vibrational contribution to the Helmholtz free energy of the system. The Helmholtz free energy *F(V, T)* of the crystal as a function of temperature and volume can be approximately is expressed by

$$F(V,T) = F_{el}(V,T) + F_{vib}(V,T)$$

$$F_{el(vib)} = U_{el(vib)} - TS_{el(vib)} \tag{8}$$

where F_{el} and F_{vib} denote the electrons and phonons contributions to the free energy, respectively. Generally, the entropy (S_{el}) contribution from electrons is negligible, and U_{el} contribution can be calculated from DFT. From QHA, F_{vib} can be written by:

$$F_{vib} = \frac{1}{2}\sum_{q,v} \hbar\omega_{q,v}(V) + K_B T \sum_{q,v} In[1 - exp(-\hbar\omega_{q,v}(V)/K_B T)] \tag{9}$$

where $\boldsymbol{q}$ and ν are the wave vector and band index, respectively; $\omega_{q,\nu}$ is the phonon frequency with a wave vector $\boldsymbol{q}$ and band ν; $\hbar$, K_B, and T denote Planck's constant, Boltzmann constant and temperature, respectively. The vibrational entropy (S_{vib}) can be calculated by

$$S_{vib} = -\left(\frac{\partial F_{vib}}{\partial T}\right)_V$$

$$= \frac{1}{2T}\sum_{q,\upsilon}\hbar\omega_{q,\nu}\coth\left(\frac{\hbar\omega_{q,\nu}}{2K_BT}\right) - K_B\sum_{q,\upsilon}\ln\left[2\sinh\left(\frac{\hbar\omega_{q,\nu}}{2K_BT}\right)\right] \quad (10)$$

The vibrational free energy and entropy of Li_3OCl have also been calculated using Eqs. (9) and (10) and plotted in Figure S1. The vibrational free energy at 0 K is the zero point energy of the system. The vibrational free energy decreases as temperature increases, whereas the entropy increases with temperature.

Figure S2 shows the calculated Helmholtz free energy of Li_3OCl using QHA (Eq. (8)). The black solid lines are the fitted curves at a given temperature ranging from 200 to 900 K, and different symbols in each curve correspond to the minimum energy and equilibrium volume. The red dash line that connects each equilibrium volumes is only for guiding eyes. It can be seen that the equilibrium volume and free energy of the system increases and decreases with temperature, respectively.

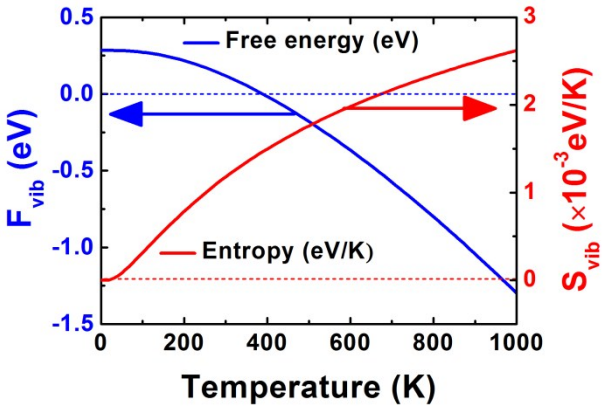

Fig. S1 Vibrational free energy and entropy of Li_3OCl as a function of temperature.

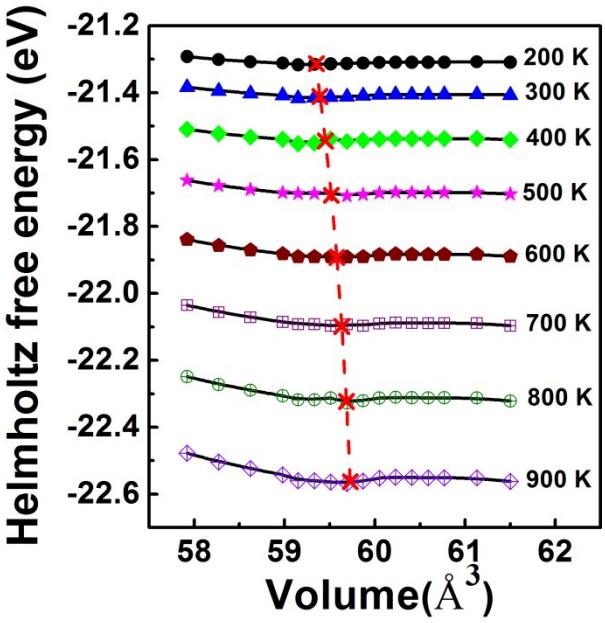

Fig. S2 Helmholtz free energy of Li_3OCl as a function of primitive cell volume at different temperatures.

Next, the volume thermal expansion coefficient (α_V) of Li_3OCl is calculated by

$$\alpha = \frac{1}{V(T)}\frac{dV(T)}{dT}, \tag{11}$$

where V is the volume of a cell.

3.2 Thermal conductivity

Generally, the thermal conductivity (κ_L) of a solid material has contributions from both electrons and phonons. As discussed above, Li_3OCl is a wide band gap insulator and heat transport through electrons can be negligibly small. Therefore, we only considered phonon contribution to thermal conductivity (κ_L) for Li_3OCl using the following Slack[14] expression

$$\kappa_L = A\frac{\bar{M}\theta_D^3\delta}{\gamma^2 n^{2/3} T}, \tag{12}$$

here n is the number of atoms in the primitive unit cell; δ is the cube root of average atomic volume; θ_D is the Debye temperature; $\bar{M}$ is the average mass of the atoms in the crystal; A is a collection of physical constants (3.1×10^{-6} if κ is in W/mK); $\bar{M}$ in atomic mass unit; δ in angstroms; γ is the Grüneisen parameter, which is a direct measure of the anharmonicity of

the bonds, and can be expressed as[15]

$$\gamma = \frac{3\alpha_V BV}{C_V}, \quad (13)$$

where α_V is the volume thermal expansion coefficient; B is the isothermal bulk modulus; V is the molar volume and C_V is the heat capacity at constant volume. To calculate the thermal conductivity, C_V and θ_D must be obtained first. The C_V can be calculated as a function of temperature using the following relations

$$C_V = -T\left(\frac{\partial^2 F_{vib}}{\partial T^2}\right)_V$$

$$= \sum_{j,k} K_B \left(\frac{\hbar\omega_{j,k}}{K_B T}\right)^2 \frac{exp(\hbar\omega_{j,k}/K_B T)}{[\exp\left(\frac{\hbar\omega_{j,k}}{K_B T}\right) - 1]^2}. \quad (14)$$

Figure S3 shows the heat capacity C_V as a function of temperature. It can be seen that at lower temperatures, C_V increases rapidly with temperatures, in proportional with T^3 and follows the typical Debye model, as shown in the insert of Figure S3. As temperature increases to 400 K, the heat capacity C_V reaches 1.17×10^{-3} eV/K, very close the Dulong-Petit limit of solid materials (1.29×10^{-3} eV/K). In addition, due to the anharmonic approximations of the Debye model used here, we can determine the Debye temperatures (θ_D) by fitting the C_V curve at the low temperature range (see insert of Figure S3) with the Debye model of the following

$$C_V = \left(\frac{12}{5\theta_D^3}\pi^4 k_B n N_A\right) T^3, \quad (15)$$

where N_A is the Avogadro constant, and n is the number of atoms in the primitive unit cell. From Eq. (15), we estimated the Debye temperature (θ_D) to be ~412.6 K through fitting with cubic polynomial C_V curve at a temperature range of 0 to 30 K.

Finally, through the obtained data from Eq. (13) to (15), the thermal conductivity (κ_L) of Li_3OCl can be calculated by using Eq. (12).

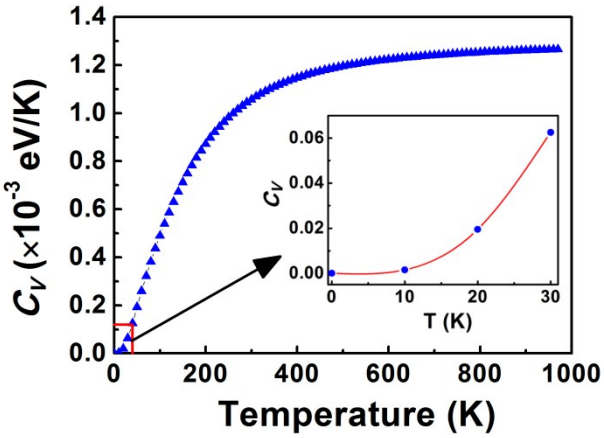

Fig. S3 Temperature-dependent specific heat at constant volume of Li_3OCl, The inset shows the typical T^3 Debye model behavior at low temperature ranging from 0 to 30 K.

4. Defect chemistry

Table S1 Energy difference of different defect configurations

Defect types	Defect sites	Defect pair distance (Å)	Energy difference (eV)
Frenkel defect (V'_{Li}-$Li^{\bullet}_{i}$)	V_1	2.763	0
	V_2	3.908	0.032
	V_3	4.786	0.071
	V_4	5.526	0.038
	V_5	6.179	0.003
	V_6	6.768	0.069
	V_7	7.311	0.100
LiCl defect (V'_{Li}-$V^{\bullet}_{Cl}$)	N_1	2.763	0.108
	N_2	4.786	0
	N_3	6.179	0.157
	N_4	7.311	0.188
Li_2O defect ($2V'_{Li}$-$V^{\bullet\bullet}_{O}$)	A_j	1.954/1.954	0
	O_p	1.954/1.954	0.007
	S_1	4.369/1.954	0.705
	S_2	5.862/1.954	0.698

O_{Cl} defect ($O_{Cl}^{'}$ - $Li_i^{\bullet}$)	T	1.819	0.118
	D_1	1.819	0
	D_2	1.777	0.012
	S	4.066	0.452

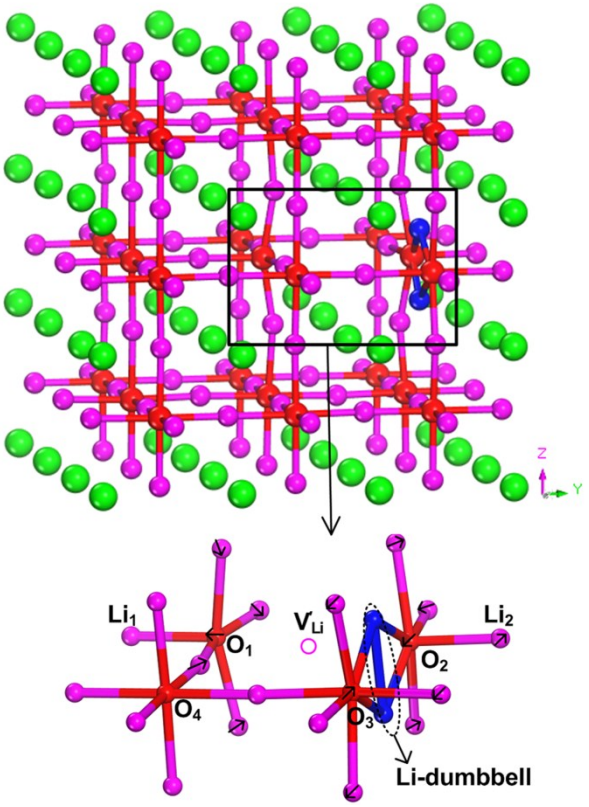

Fig. S4 The most-stable structure of the Frenkel defect in the 3×3×3 supercell and the local structure around the Li vacancy and interstitial Li-Li dumbbell.

Figure S4 shows the lowest energy configuration (V_1) in the Frenkel defect case (d). For the surrounding $V_{Li}^{'}$, these are dominated by the motion of the nearest-neighbor O anion (labeled as O_1 and O_2 in Figure S4). The bond length of O_1-O_2 is increase by ~0.316 Å, in contrast to the defect-free system (O-O bonding ~3.908 Å) due to Coulombic repulsion. This directly results in a shortening of the O_1-Li_1 and O_2-Li_2 bonds by ~0.127 Å and ~0.077 Å, respectively. Moreover, the nearest-neighbor Li^+ moves toward $V_{Li}^{'}$ due to the Coulombic attraction, and the remaining four O-Li bonds are shortened by an average of ~0.053 Å,

compared to the defect-free system (O-Li bond 1.954 Å) in the $[O_1Li_5]$ square pyramids. For interstitial Li-Li dumbbells surroundings, the additional Li atom shares a vertex with another Li in a Li_6O octahedron, which thus has to move away from the vertex of the octahedron and forms a Li_7O polyhedron. Moreover, the two Li atoms form a Li-Li dumbbell that is centered on the original Li site and oriented parallel to the edges of the Li_6O octahedron. Compared to the perfect crystal, the nearest-neighbor O atoms (O_2 and O_3 in Figure S4) move toward the Li dumbbell by ~0.474 Å due to Coulombic attraction. Conversely, the near-neighbor Li atoms shifted away from the Li dumbbell, which results in the Li-O bond. However, Li_2-O_2 distance is increased by an average of 0.104 Å in the polyhedron made of O_2, O_3, and Li atoms. The Cl atoms and other Li-O bond (such as O_4-Li in Figure S4) that are far away from the defect in the supercell do not change. It indicates that the defect ($V_{Li}^{'}$ or $Li_i^{\bullet}$) only gives rise to a local atomic and geometric structure change, which is consistent with the ionic nature of the material. The results is in good agreement with those by Stegmaier *et al*. [16]

5. Discussions on Li^+ migration mechanisms

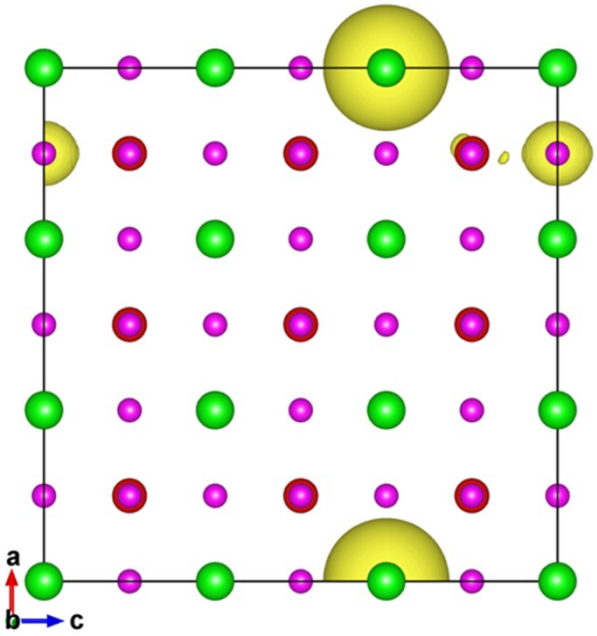

Fig. S5 Differential charge density of LiCl defect pair case in 3×3×3 Li_3OCl supercell. The yellow contour represents the charge distribution, and the value of isosurface is set to be 0.1 e/Å^3.

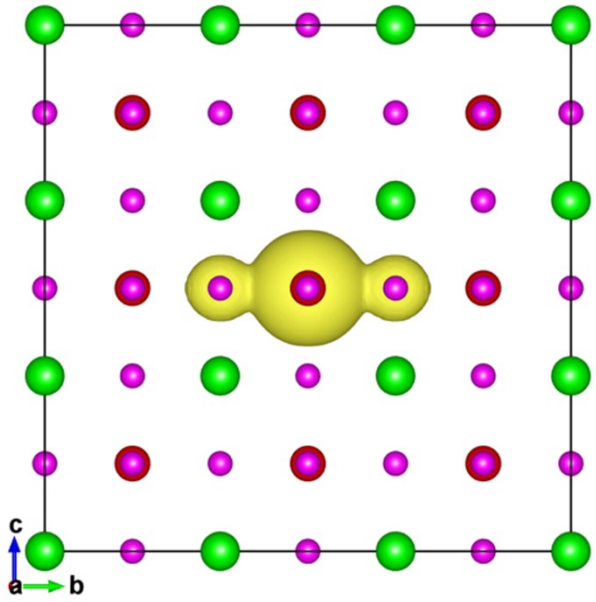

Fig. S6 Differential charge density of Li_2O defect pair case in 3×3×3 Li_3OCl supercell. The yellow contour represents the charge distribution, and the value of isosurface is set to be 0.1 e/Å^3.

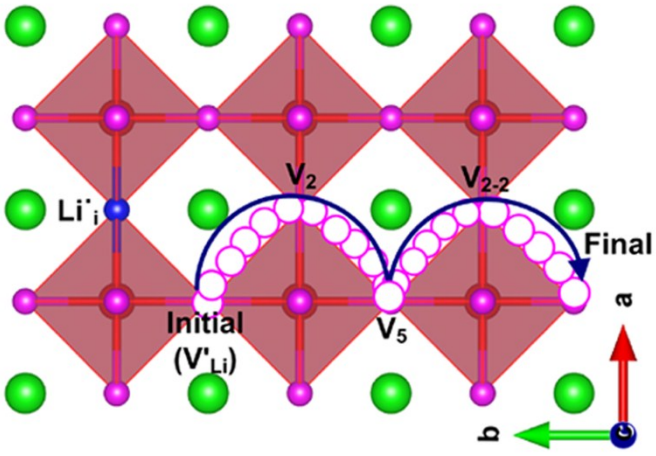

Fig. S7 Schematic drawing of the migration pathway of $V_{Li}^{'}$ in the Frenkel defect case

In the diffusion pathway, a $V_{Li}^{'}$ moves to the periodic image after a four-step migration: initial state (V_1)→V_2→V_5→$V_{2\text{-}2}$→final state (V_1).

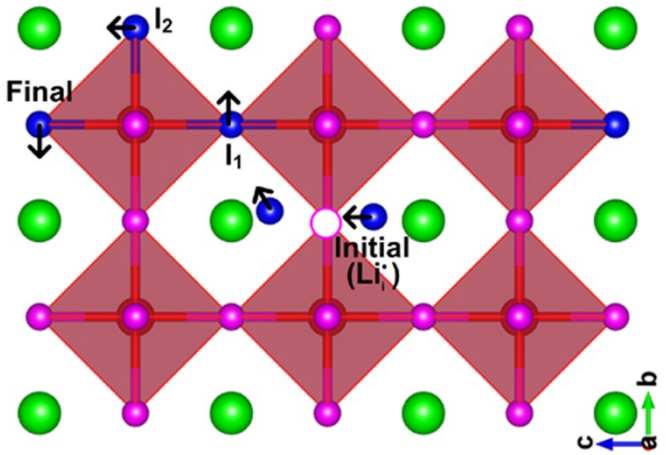

Fig. S8 Schematic drawing of the migration pathway of $Li_i^{\bullet}$ in the Frenkel defect case

Notes and References

1 H. J. Monkhorst and J. D. Pack, *Phys. Rev. B***,** 1976, **13**, 5188-5192.

2 A. V. Krukau, O. A. Vydrov, A. F. Izmaylov and G. E. Scuseria, *J.Chem. Phys.*, 2006, **125**, 224106.

3 Y. S. Kim, K. Hummer and G. Kresse, *Phys. Rev. B*, 2009, **80**, 035203.

4 A. Togo and I. Tanaka, *Scr. Mater.*, 2015, **108**, 1-5.

5 X. Gonze and C. Lee, *Phys. Rev. B: Condens. Matter Mater. Phys.*, 1997, **55**, 10355.

6 G. Henkelman, B. P. Uberuaga and H. A. Jónsson, *J. Chem. Phys.***,** 2000, **113**, 9901.

7 J. T. Wang, C. F. Chen and Y. Kawazoe, *Phys. Rev. Lett.*, 2011, **106**, 075501.

8 Z. J. Wu, E. J. Zhao, H. P. Xiang, X. F. Hao, X. J. Liu and J. Meng, *Phys. Rev. B*, 2007, **76**, 054115.

9 W. Voigt, *New York: Macmillan,* 1928, pp, 313-315.

10 A. Reuss and Z. Angew, *Math. Mech.*, 1929, **9**, 49-58.

11 R. Hill, *Proc. Phys. Soc., London, sect. A*, 1952, **65**, 349-354.

12 S. F. Pugh, *Philos. Mag. Ser.*, 1954, **45**, 823-843.

13 D. H. Chung and W. R. Buessem, *J. Appl. Phys.*, 1967, **38**, 2010-2012.

14 G. A. Slack, *Solid State Phys*., 1979, **34**, 1-71.

15 D. T. Morelli, V. Jovovic and J. P. Heremans, *Phys. Rev. Lett.*, 2008, **101**, 035901.

16 S. Stegmaier, J. Voss, K. Reuter and A. C. Luntz, *Chem. Mater.*, 2017, **29**, 4330-4340.